nature physics

SUPPLEMENTARY INFORMATION

DOI: 10.1038/NPHYS1508

Self-organized adaptation of simple neural circuits enables complex robot behavior

Silke Steingrube[1,2], Marc Timme[1,3,4], Florentin Wörgötter[1,4] and Poramate Manoonpong[1,4,*]

[1] Bernstein Center for Computational Neuroscience, 37073 Göttingen, Germany
[2] Department of Solar Energy, Institute for Solid State Physics, ISFH / University of Hannover, 30167 Hannover, Germany
[3] Network Dynamics Group, Max Planck Institute for Dynamics & Self-Organization, 37073 Göttingen, Germany
[4]Faculty of Physics,University of Göttingen, 37077 Göttingen, Germany
Emails: silke@bccn-goettingen.de, timme@chaos.gwdg.de, worgott@bccn-goettingen.de, poramate@bccn-goettingen.de

∗ To whom correspondence should be addressed. E-mail: poramate@bccn-goettingen.de

Ref: NPHYS-2009-04-00611B

This supplementary information includes:

- **Materials and methods** describing the biomechanical setup of the AMOS-WD06 system and its neural control
- **Performance of the AMOS-WD06 system** demonstrating robot walking experiments with neural control
- **Supplementary figures 1-7**
- **References**
- **Supplemental video legends 1-6**
- **Supplementary videos 1-6**

DOI: 10.1038/NPHYS1508

1 Materials and methods

The first section describes the biomechanical setup of the six-legged walking machine "AMOS-WD06", followed by details of the sensor-driven neural controller and its sub-modules.

1.1 The six-legged walking machine AMOS-WD06 (Biomechanics)

The six-legged walking machine AMOS-WD06[1] (Supplementary Figure 1A,B) is a hardware platform for studying the coordination of many degrees of freedom, for performing experiments with neural controllers, and for the development of artificial perception-action systems employing embodied control techniques.

It consists of a two-part body connected by one backbone-joint (BJ), at which six identical legs and one tail are attached. Each leg has three joints (three degrees of freedom) that are controlled by electro-motors: the thoraco-coxal (TC-) joint enables forward (+) and backward (−) movements, the coxa-trochanteral (CTr-) joint enables elevation (+) and depression (−) of the leg, and the femur-tibia (FTi-) joint enables extension (+) and flexion (−) of the tibia (Supplementary Figure 1B). The morphology of these multi-jointed legs is modelled on the basis of a cockroach leg (Supplementary Figure 1C,D and see (1) for more details) but the tarsus segments are ignored. Each tibia contains a spring compliant element to absorb impact force as well as to measure ground contact during walking.

The body of AMOS-WD06 consists of two segments: a front segment where two forelegs are installed and a central body segment where the two middle and the two hind legs are attached. They are connected by one active backbone joint inspired by the invertebrate morphology of the American cockroach's trunk (Supplementary Figure 1 and see (2) for more details). This backbone joint is for up- and downward bending, which allows the walking machine to climb over obstacles. The applications of the neural chaotic controller presented here and in the main manuscript text keep this joint fixed; however, the application is readily extended to also use this joint[2]. All leg joints are driven by analog servomotors, while the backbone joint is driven by a digital one. The size of the walking machine is 30 cm wide, 40 cm long, 12 cm high without its tail. The length of the tibiae is 10 cm. They are attached to the FTi-joints, roughly resembling the length of real tibiae

[1] Advanced MObility Sensor driven-Walking Device 06.

[2] For autonomous climbing over obstacles, we refer the reader to the video clip at http://www.manoonpong.com/AMOS/Climbing/AMOSclimbing.mpg. Note that describing the controller of this climbing behavior developed based on the proposed sensor-driven neural controller will go beyond the scope of this article.

in relative size compared to the total machine. The weight of the fully equipped robot (including 21 servomotors, all electronic components, sensors, and a mobile processor) is approximately 4.2 kg. Electrical power supply is provided by batteries.

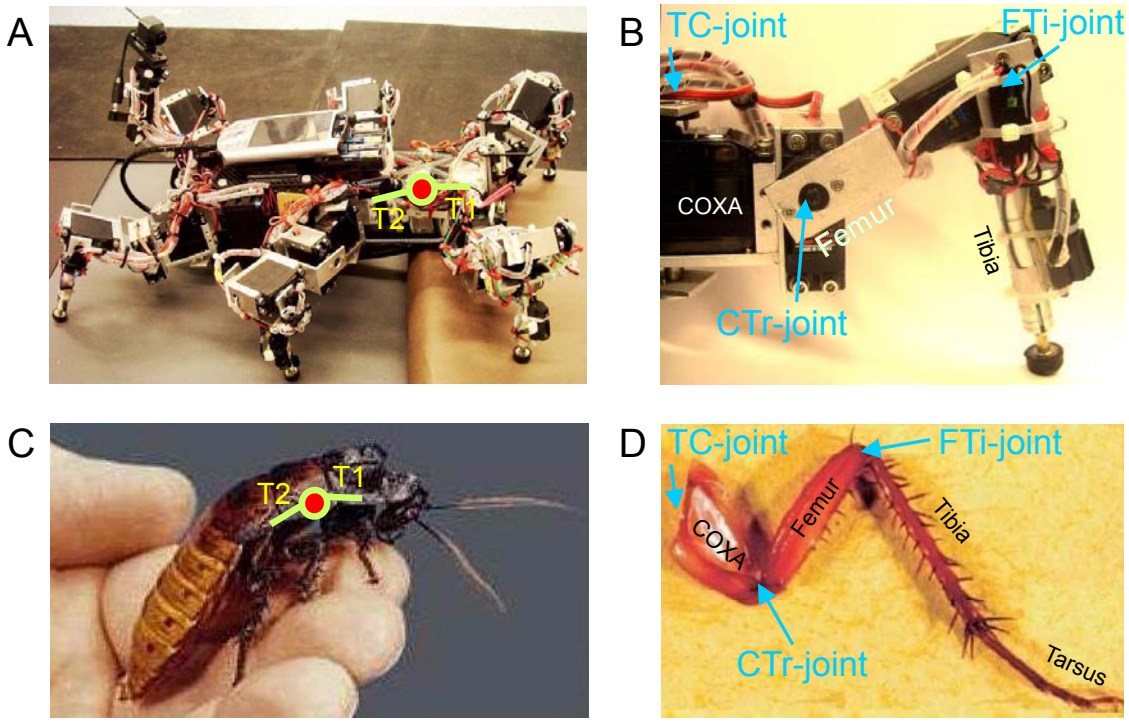

Supplementary Figure 1: **The six-legged walking machine AMOS-WD06 inspired by the morphology of the American cockroach.** **(A)** Climbing position of AMOS-WD06 with a body flexion joint. **(B)** The physical leg with three degrees of freedom of AMOS-WD06. **(C)** Climbing position of a cockroach. It can bend its trunk downward at the joint between the first (T1) and second (T2) thoracic segment to keep the legs close to the surface of an object for an optimum climbing position and even to prevent unstable actions (modified from (3)). **(D)** Cockroach leg (modified from (4)).

Our walking machine has all in all 20 sensors (see Fig. 1 of the main manuscript text) for controlling various reactive and adaptive behaviors. The control of this walking machine is kept on a simple but powerful board, the Multi-Servo IO-Board (MBoard), which is capable of controlling up to 32 motors, and receiving up to 36 analog sensor inputs; its size is 125 mm x 42 mm x 15 mm. The MBoard can be interfaced with a personal computer (PC) or a personal digital assistant (PDA) via a RS232 serial connection at 57.6 kbits/s. Note that for robot experiments we implement the controller on the PDA where

DOI: 10.1038/NPHYS1508

we are, due to the firmware of the PDA, forced to use an update frequency of the whole system of 38 Hz (26 ms cycle time). However, this is too fast for the motors. Therefore we just skip several periods of the neural CPG controller to arrive at a down-sampled signal. If not for the restrictions imposed by us from this PDA, normally one would just choose a slow sampling frequency to begin with and then arrive at a 1:1 mapping without having to perform this skipping procedure. In a natural system with analogue operating neurons such problems do not exist.

1.2 Processing Network

1.2.1 Overview

The complete processing network consists of the novel controller and some other standard pre- and post-processing modules needed for signal shaping described in the following. All pre- and post-processing modules are generic and have been used also in other (e.g., four- and eight-legged) walking machines (2; 5). Essentially these modules perform filtering, amplitude modulation and phase-shifting of the control signal to allow for the coordination of the different legs. Their parameters are non-critical and robustness analyzes can be found in older studies (2; 5). Furthermore, these modules are abstractions from those found in real insects (6; 7).

Supplementary Figure 2 shows the detailed setup of sensor-driven neural control consisting of five main modules (neural preprocessing module (pink units, Supplementary Figure 2A), adaptive neural chaos control module (B, yellow units), neural CPG postprocessing module (C, green units), neural motor control module (D, orange units), and a delay line circuit for sequencing the motor signals for the different legs (D, blue units). A coarse view of this is displayed in Fig. 1 of the main manuscript text.

1.2.2 (A): Sensors and Neural Preprocessing Module

All raw sensory data used to provide environmental information for our sensor-driven robot system are fed into a neural preprocessing module having several subnetworks for orienting and gait preprocessing (pink units in Supplementary Figure 2A).

Sensors for orienting behavior: We use infra-red ($IR_{1,2,3,4}$) together with light dependent resistor ($LDR_{1,2}$) sensor signals to trigger different types of tropisms, e.g., obstacle avoidance behavior (negative tropism, see Supplementary Video 3) and phototaxis (positive tropism, see Supplementary Video 3). An upside-down detector sensor signal (UD) serves to activate a self-protective reflex behavior by inhibiting all motor neurons when the machine is turned into an upside-down position (Supplementary Video 3).

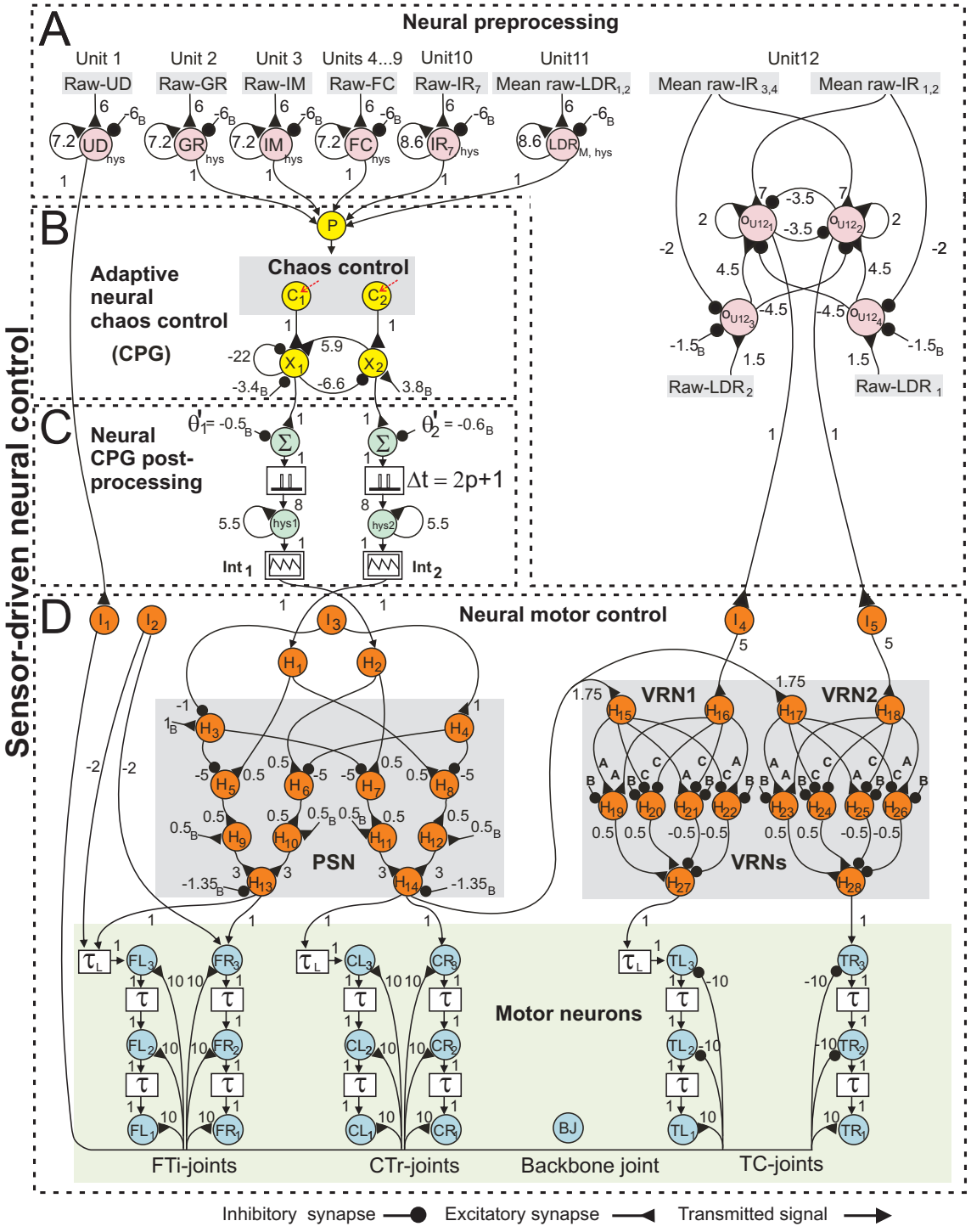
A
Neural preprocessing
Unit 1
Raw-UD
Unit 2
Raw-GR
Unit 3
Raw-IM
Units 4...9
Raw-FC
Unit10
Raw-IR7
Unit11
Mean raw-LDR1,2
Unit12
Mean raw-IR 3,4
Mean raw-IR 1,2
B
Adaptive neural chaos control (CPG)
Chaos control
C
Neural CPG post-processing
Int 1
Int 2
Raw-LDR2
Raw-LDR 1
Sensor-driven neural control
D
Neural motor control
VRN1
VRN2
PSN
VRNs
Motor neurons
FTi-joints
CTr-joints
Backbone joint
TC-joints
Inhibitory synapse
Excitatory synapse
Transmitted signal

DOI: 10.1038/NPHYS1508

Supplementary Figure 2: **Sensor-driven neural control.** It generates stimulus induced behavior of AMOS-WD06 by means of adaptive neural chaos control (see text for details). Parameters are A = 1.7246, B = -2.48285, C = -1.7246. **(A) Neural preprocessing module**: UD_{hys} = hysteresis neuron of the upside-down detector sensor signal (unit 1); GR_{hys} = hysteresis neuron of the gyro sensor signal (unit 2); IM_{hys} = hysteresis neuron of the inclinometer sensor signal (unit3); FC_{hys} = six hysteresis neurons of the foot contact sensor signals (units 4,...,9); $\text{IR}_{7,hys}$ = hysteresis neuron of the rear infra-red sensor signal (unit 10); $\text{LDR}_{M,hys}$ = hysteresis neuron of the mean value of the left and right light dependent resistor sensor signals (unit11); $o_{U12_{1,2}}$ = output neurons and $o_{U12_{3,4}}$ = hidden neurons of the preprocessing unit (unit 12) of the light dependent resistor sensor signals and the infra-red sensor signals coming from the sensors implemented at the front part ($\text{IR}_{2,3}$) and at the front legs ($\text{IR}_{1,4}$). Note that only one foot contact sensor signal with its neural preprocessing (FC) is presented while others, having the same setup, are omitted. **(B) Adaptive neural chaos control module**: p = target period; $c_{1,2}$ = self-adapting signals; $x_{1,2}$ = output neurons of the CPG network. **(C) Neural CPG postprocessing module**: Δt = time window function; $\text{hys}_{1,2}$ = hysteresis neurons; Int = integrator units. **(D) Neural motor control module**: $I_{1,\ldots,5}$ = neural control parameters for generating omnidirectional walking behavior; $H_{1,\ldots,14}$ = interneurons of the PSN; $H_{15,\ldots,28}$ = interneurons of the VRNs. **Motor neurons**: TR_1, CR_1, FR_1 = TC-, CTr- and FTi-motor neurons of the right front leg (R1); TR_2, CR_2, FR_2 = right middle leg (R2); TR_3, CR_3, FR_3 = right hind leg (R3); TL_1, CL_1, FL_1 = left front leg (L1); TL_2, CL_2, FL_2 = left middle leg (L2); TL_3, CL_3, FL_3 = left hind leg (L3); BJ = a backbone motor neuron which is here deactivated; i.e., it stays in a fixed position. All numbers marked with subscript "B" refer to bias terms. The location of the motor neurons and sensor neurons on the AMOS-WD06 is presented in Fig. 1 of the main manuscript text. Note that in general the FTi-joints are inhibited; i.e., they stay in a flexed position. When a leg is losing ground contact the FTi-joint of this leg will be activated by the chaotic signal.

Sensors for walking behavior: We use foot contact ($FC_{1,\ldots,6}$), gyro (GR), inclinometer (IM), light dependent resistor ($LDR_{1,2}$), and infra-red (IR_7) sensor signals to determine the walking period p (see below).

Pre-processing: All raw sensory signals require preprocessors to eliminate the sensory noise as well as for shaping the sensory data. In the application presented here, twelve neural preprocessing units utilize the dynamic properties of recurrent neural networks. Eleven neural preprocessing units are built as single hysteresis elements (see ref. (8)). The hysteresis principle (2; 8) leads to a nonlinear transition of two output states (low and high activation). Thus, hysteresis units can effectively filter sensory noise and control the duration in response to stimuli from the environment. A twelfth unit is derived from a minimal recurrent controller (MRC) structure (9) which allows balancing positive (LDR) and negative (IR) tropisms leading to a final resulting turning signal processed to the VRNs. As a result, the walking machine can effectively perform an appropriate turning angle to avoid obstacles or corners as well as turn toward a light source. All neural preprocessing parameters, e.g., synaptic strengths and bias terms (see Supplementary Figure 2A) were found by experiments (see (5; 10) for more details of the neural preprocessing parameters).

1.2.3 (B): Adaptive neural chaos control module (CPG)

The pre-processed signals from the sensors for walking behavior are then combined and the result is fed into the chaotic controller (yellow units in Supplementary Figure 2B) that performs as the central pattern generator (CPG). As described in the main text of the manuscript, the parameters of the two-neuron control module are initially adjusted such that its dynamics is chaotic if uncontrolled. The preprocessed sensory-signals determine an integer number p, which is the desired output period of the CPG signal. This is achieved either via error-minimization in a learning process (see main text as well as Sect. 2 below) or – as a shortcut – by using a pre-defined sensor-to-period mapping according to Table 1 in the main text. The CPG output becomes p-periodic by using the novel adaptive neural chaos control method (see also main text) to stabilize originally unstable period orbits that are embedded in the chaotic attractor of the module. We remark that chaos on the one hand serves as a ground state of the CPG module, on the other hand it is also functionally used for self-untrapping.

1.2.4 (C): Neural CPG postprocessing module

The output of both neurons of the controlled CPG is sent to a postprocessing module (green units in Supplementary Figure 2C). In this postprocessing module, the signals are smoothed, employing recurrent hysteresis neurons, and integrated in an integrator unit (Int, see Supplementary Figure 2C).

DOI: 10.1038/NPHYS1508

Specifically, the neural CPG postprocessing module consists of three hierarchical subunits: i) time window function units Δt for setting an appropriate number of iteration steps which correspond to the cycle for updating the CPG signal, ii) hysteresis units $hys1, 2$ for signal shaping, and iii) signal integrator units $Int1, 2$ to obtain continuous ascending and descending motor signals. Supplementary Figure 3 shows CPG signals after postprocessing by each unit.

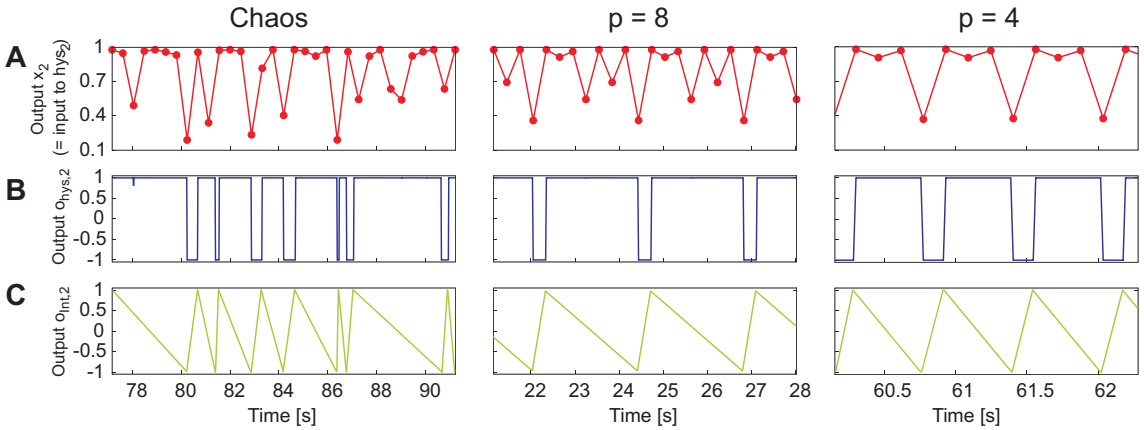

Supplementary Figure 3: **Postprocessing signals for different periods.** **(A)** Output signals of the time window function unit Δt. **(B)** Output signals of the hysteresis unit $hys2$. **(C)** Output signals of the signal integrator unit $Int2$.

1.2.5 (D): Neural motor control modules

Subsequently, the post-processed CPG outputs are transmitted to the neural motor control module (orange and blue units in Supplementary Figure 2D). The orange units describe one phase switching network (PSN, (5)) and two velocity regulating networks (VRNs, (2; 5)). The blue units represent delay lines (5).

The PSN is a generic feed-forward network, which reverses the phase of the periodic signals driving the CTr- and FTi-joints. As a consequence, these periodic signals can be switched to lead or lag behind each other by $\pi/2$ in phase in accordance with the given input I_3. The PSN has been implemented to allow for sideways walking, e.g., for obstacle avoidance (see (5) for more details on parameters and specific experiments on sensor-driven sideways walking).

The two VRNs are also simple feed-forward networks (see (2)). Each VRN controls the three ipsilateral TC-joints on one side. Because the VRNs behave qualitatively like a

multiplication function (2), they have capability to increase or decrease the amplitude of the periodic signals by the magnitude of the inputs $I_{4,5}$. Consequently, the walking velocity of the machine will be regulated, i.e., the higher the amplitude of the signal the faster it walks (not shown in the current set of experiments but see (2)). Furthermore they can be used to achieve more walking directions, like forward and backward movement (sign inversion of the multiplication) or turning left or right where the directions are driven by the preprocessed infra-red and light dependent resistor sensor signals through $I_{4,5}$.

At the blue delay line units, delays τ_L between the output of the motor control module and the rear left leg joints are used. These delays are independent of the target period or other influences. The described setup leads to biologically motivated leg coordination since the legs on each side perform phase shifted waves of the same frequency (11). The ipsilateral lag is determined by τ and the phase shift between both sides is given by τ_L. The frequency of the waves is defined by the target period of the chaos control network.

2 Performance of the AMOS-WD06 system: Additional Experiments and Videos

Here several more walking experiments are presented that complement those shown in the main manuscript text.

Basic, predefined behaviors: As mentioned, learning as well as pre-wiring (using Table 1 from the main manuscript text) can be used to determine the different behaviors of our hexapod. The following aspects are shown using a pre-defined mapping:

1. Examples of different gaits (Supplementary Video 1 and Supplementary Figure 4). This shows in a clear and separated way the different gaits which can appear (intermixed) during walking in complex terrain.

2. Autonomous selection of different gaits and other complex behaviors achieved by sensor-driven triggering of different pre-defined target periods without learning (Supplementary Video 2 and Supplementary Figure 4, see also Fig. 3 of the main manuscript text). Gyro (GR) and inclinometer (IM) signals lead to faster or slower gaits depending on the slope. Foothold search using chaotic motion triggered by a lack of ground contact. Phototaxis is induced by the LDR-sensor signal being larger than a predefined threshold. This selects target period $p = 4$ leading to a fast tripod gait. Resting behavior (target period $p = 1$) is triggered by a too strong light at LDR.

3. Positive photo-tropism and negative tropism away from an obstacle (Supplementary Video 3, see also Supplementary Video 2). Motor signals of these asymmetric

DOI: 10.1038/NPHYS1508

behaviors, indicative of the actions of the PSN and VRN networks, are shown in Supplementary Figure 5).

4. Escape behavior, triggered by the infra-red rear sensor and leading to target period $p = 4$, a fast tripod gait (simulated predator attack, Supplementary Video 3).

5. Protective reflex triggered by the upside-down detector (UD) is also shown in Supplementary Video 3.

6. Detailed rendering of a foothold-searching experiment (Supplementary Video 4 and Supplementary Figure 6). This shows how chaos can actually be exploited in a behavioral context for untrapping, where periodic foothold search (no chaos) will not succeed.

Learned behaviors: One of the main aspects of this work is to show that the centralization of control via our novel adaptive CPG leads to the unique situation that the learning of a sensor-motor mapping becomes exceedingly simple, because it is channelled only through this controller not having to involve any other network structures. To support this notion several different learning experiments have been performed, some of which are shown here:

1. Learning to select an energy saving gait (Supplementary Video 5 and Fig. 4 in the main manuscript text). This experiment is described in detail in the main text. The robot uses the energy uptake as an error signal for the learning of the mapping between terrain inclination and gait-type.

2. Learning to escape danger from behind. In this experiment the robot learns to select a fast gait from a "danger from behind" error signal (Supplementary Video 6 and Supplementary Figure 7). We use an auditory-wind detector sensor (AW) (12) and a rear infra-red sensor (IR_7) for detecting distant sounds at AW (made by an approaching predator) and too near, hence potentially dangerous, approaching objects at IR from behind. The learning mechanism is similar to the one described in the main manuscript text (see Fig. 4 of the main manuscript text) where the IR signal is used to generate an error signal e while the sound signal is the sensory signal which provides the appropriate to-be-learned correlation. Before learning the robot selects the fast gait only in response to the (too-near) IR-signal. After learning, it selects it already when "hearing" the approaching predator this way triggering an earlier escape reaction.

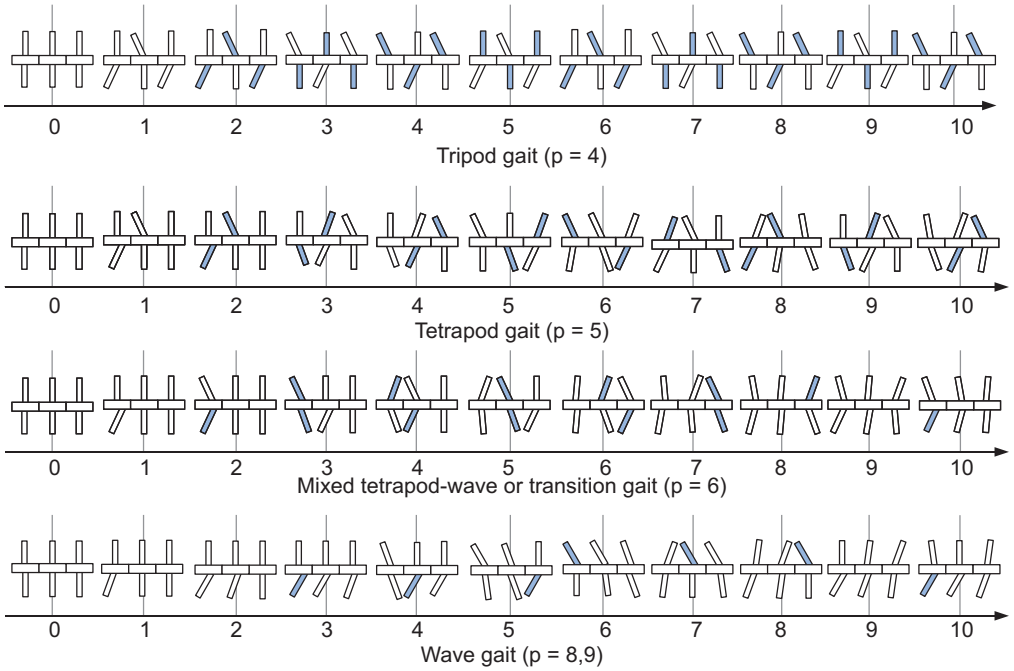

Supplementary Figure 4: **Sketch of different walking patterns according to target periods p.** A blue colored leg is in the air, a white leg is on the ground. To keep the images concise, only very coarse schemes are shown that do not take into account the different timings of swing and stance phases.

DOI: 10.1038/NPHYS1508

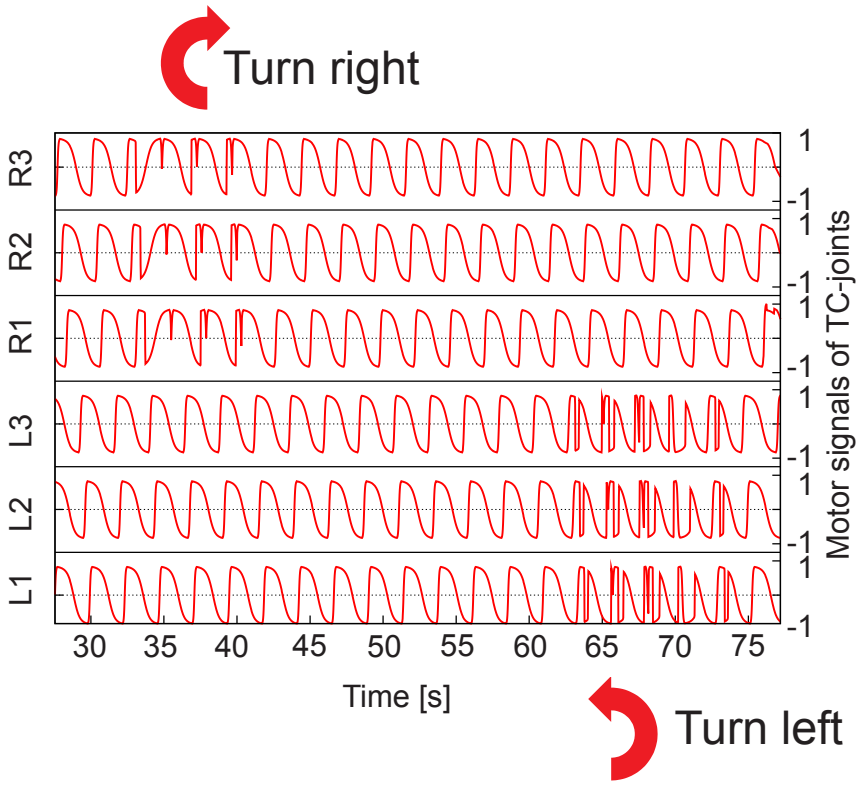

Supplementary Figure 5: **Obstacle avoidance using orienting responses.** The TC-joint signals of all six legs. At first, the walking machine avoids obstacles on its left by turning to the right and it returns to forwards walking as soon as obstacles are not any longer detected (at around time $t = 40s$). At around $t = 65s$, there are obstacles on its right. As a result, it turns left. For right turning, the inversion of the right TC-signals is clearly visible. Hence, the right legs perform a forward stance and backward swing phase which results in a right turn. For the left turn, the motor signals of the left legs appear perturbed and the inversion is not so clearly visible. This results from short time intervals during which the sensors do not detect obstacles and the walking machine tries to walk straight. Nevertheless, it performs the left turn successfully. Such inversions of the motor signals can be also observed when the machine performs phototaxis.

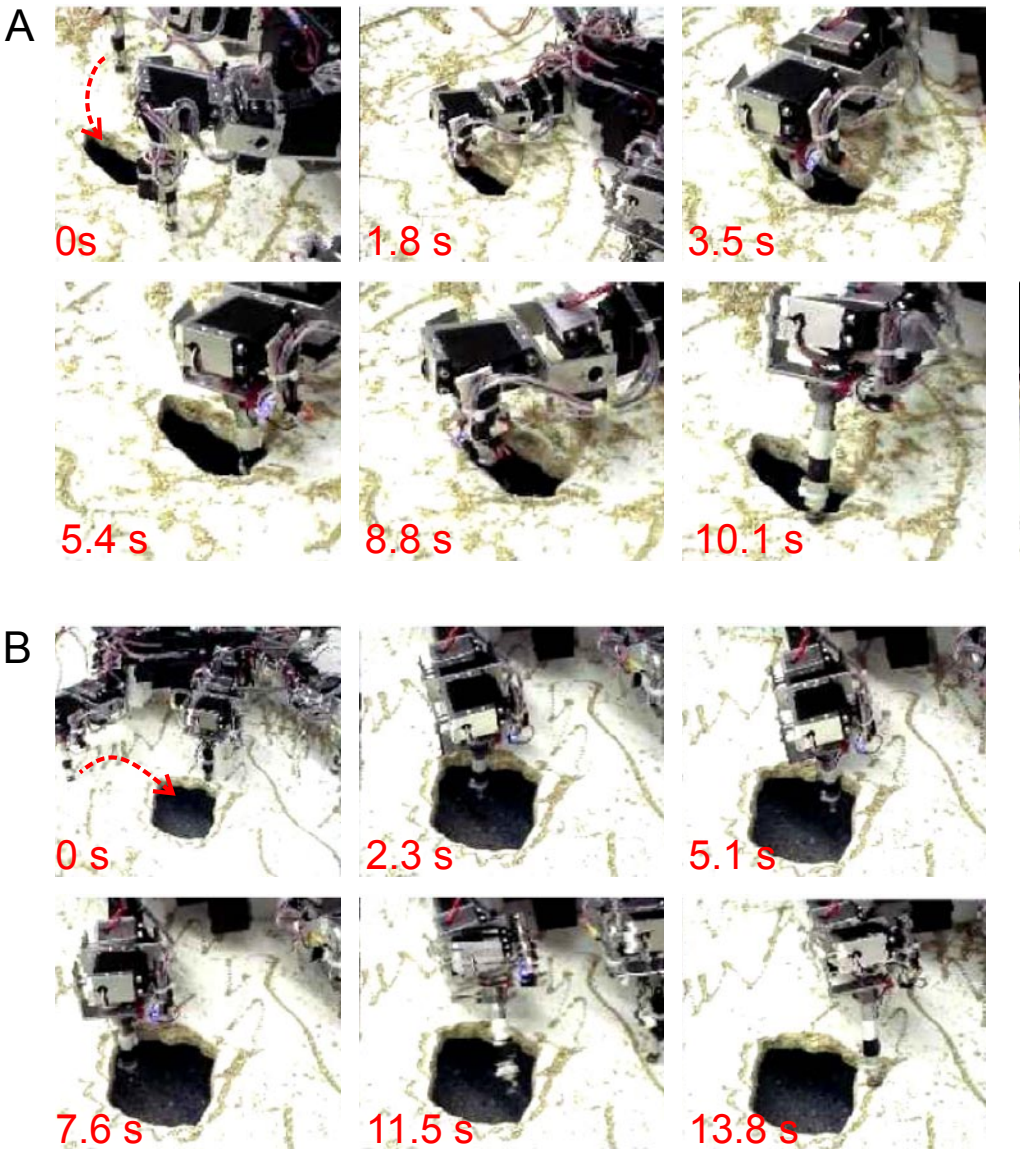

Supplementary Figure 6: **Two examples of sensor-driven foothold searching using chaos.** **(A)** Leg R3 in a small hole (first hole in Fig. 3 of the main manuscript text). **(B)** Leg R3 in a big hole (second hole in Fig. 3 of the main manuscript text). In both cases, the walking machine can perform self-untrapping in about 10-14 s. Time is shown in the lower left corner of each photo. Note that the self-untrapping is a result of an omnidirectional search pattern, i.e., for-, back-, up-, down-, and also sideways movement including the amplitude amplification of leg motion.

DOI: 10.1038/NPHYS1508

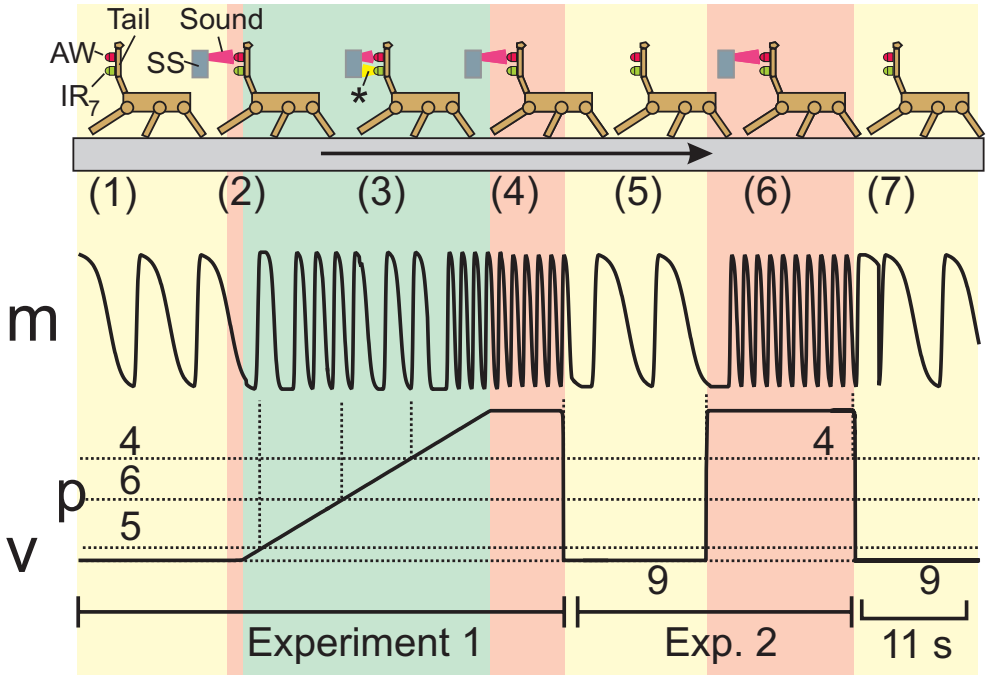

Supplementary Figure 7: **Learning to escape danger from behind.** See also Supplementary Video 6. Sound is detected by an auditory-wind detector sensor (AW) while the object is detected by the rear infra-red sensor (IR_7). In the first experiment the robot initially walks with the slow wave gait (1) and then learns [(2),(3),(4)] choosing the fast gait (tripod gait, $p = 4$) in order to speedily walk away from the too-near object (escaping danger). This leads to a drop of the infra-red signal, which is used to calculate the error signal (4) for learning. As soon as it is far enough from the object the robot then returns to its normal wave gait [(5),(7)]. In this process the correlation between AW and IR signals is being learned. Thus, in the second experiment presenting the sound (6) leads directly to the selection of the fast tripod gait requiring no further learning. The selection of period p from the output of learner neuron v follows a randomly chosen (!) mapping $v \leftrightarrow p$ shown by the dashed grid lines. Other periods (e.g., $p = 1, 8$), which were not selected, are not depicted. Learning will, regardless of this mapping, always select the "zero-error gait" (here the tripod gait). Evaluation of the speed of each gait is calculated by means of the derivative of motor signals. Symbols: m = motor signal of a TC-joint, v = output of a learner neuron, $*$ = detecting the sound source. Color code: yellow = normal forward walking situation with a slow wave gait, red = detecting low frequency sound (300 Hz) from behind, green = detecting the sound and a close object (sound source, SS) from behind.

References

[1] Ritzmann RE, Büschges A (2007) Insect walking: From reduced preparations to natural terrain, in: G. North, R.J. Greenspan (Eds.), Invertebrate Neurobiology, Cold Spring Harbor Laboratory Press.

[2] Manoonpong P (2007). Neural preprocessing and control of reactive walking machines: Towards versatile artificial perception-action systems, in: Cognitive Technologies, Springer.

[3] URL http://profootballtalk.com/HissingCockroach.jpg.

[4] Zill S, Schmitz J, Büschges A (2004) Load sensing and control of posture and locomotion, Arthropod Struct. Dev. **33**, 273–286.

[5] Manoonpong P, Pasemann F, Wörgötter F (2008) Sensor-Driven neural control for omnidirectional locomotion and versatile reactive behaviors of walking machines, Robot. Auton. Syst. **56(3)**, 265–288.

[6] Pearson KG, Iles JF (1973) Nervous mechanisms underlying intersegmental coordination of leg movements during walking in the cockroach, J. Exp. Biol. **58**, 725–744.

[7] Gabriel JP, Büschges A (2007) Control of stepping velocity in a single insect leg during walking, Philos. T. Roy. Soc. A **365**, 251–271.

[8] Pasemann F (1993) Dynamics of a single model neuron, Int. J. Bifurcat. Chaos **2**, 271–278.

[9] Pasemann F, Hülse M, Zahedi K (2003) Evolved neurodynamics for robot control, Proc. of European Symposium on Artificial Neural Networks **2**, 439–444.

[10] Manoonpong P, Pasemann F, Wörgötter F (2007) Reactive neural control for phototaxis and obstacle avoidance behavior of walking machines, Int. J. Mech. Syst. Sci. Eng. **1(3)**, 172–177.

[11] Wilson DM (1966) Insect walking, Annu. Rev. Entomol. **11**, 103–122.

[12] Manoonpong P, Pasemann F, Wörgötter F (2008) Neural preprocessing of auditory-wind sensory signals and modular neural control for auditory- and wind-evoked escape responses of walking machines, Proc. of the 2008 IEEE International Conference on Robotics and Biomimetics, 786–793.

DOI: 10.1038/NPHYS1508

Supplemental video legends:

Supplementary Video 1: **Examples of five different gaits**. Slow wave gait ($p = 9$), fast wave gait ($p = 8$), mixed tetrapod-wave or transition gait ($p = 6$), tetrapod gait ($p = 5$), and tripod gait ($p = 4$).

Supplementary Video 2: **Autonomous walking behaviors in different environmental conditions**. A complex sequence of eight different behaviors is shown that include standard walking in a tetrapod gait, up-slope walking in a wave gait, rough-terrain walking in a wave gait, self-untrapping through chaotic motion, down-slope walking in a mixture or transition gait (from wave to tetrapod), active phototaxis by fast walking in a tripod gait, and resting. As soon as obstacles are detected the machine performs obstacle avoidance behavior by turning left/right.

Supplementary Video 3: **Sensor-driven behavioral patterns**. In the first scenario, the walking machine tries to escape from the attack of a manually controlled robot by increasing its walking speed by means of changing its gait from a wave gait to a tripod gait. In the second scenario, the walking machine shows orienting responses by avoiding obstacles and performing phototaxis. Note that in this scenario it is set to walk with only one gait type (tripod gait) in order to see the orienting behavior more clearly. Furthermore, here we show that stopping the machine in front of a light source during phototaxis can be achieved by inhibiting only all TC-joints. As a result, it performs "marching" in front of the light source. In the last scenario, the walking machine performs a self-protective reflex by standing upside-down when it is turned into an abnormal walking position and it immediately returns to walk again as soon as it is turned back to its normal walking position.

Supplementary Video 4: **Foothold searching experiment with and without chaos**. When applying chaos, the walking machine successfully performs self-untrapping if its foot gets stuck in a hole but without chaos it fails.

Supplementary Video 5: **Learning to optimize energy consumption during walking on a steep slope**. The walking machine learns to search for an energy saving gait (i.e., slow wave gait) while walking on a steep slope.

Supplementary Video 6: **Learning to escape danger from behind**. The walking machine learns to search for a fast gait (i.e., tripod gait) in order to escape danger from behind. Here the low frequency sound and the reflex infra-red signal are thought to represent danger signals. They are detected by the auditory-wind detector sensor (AW) and the rear infra-red sensor (IR).